Solution and Solid Hexahydro-1,3,5-trinitro-1,3,5-triazine (RDX) Ultraviolet (UV) 229 nm Photochemistry

Katie L. Gares, Sergei V. Bykov, Thomas Brinzer, Sanford A. Asher*

University of Pittsburgh, Department of Chemistry, 4200 Fifth Avenue, Pittsburgh, PA 15260 USA

We measured the 229 nm deep-ultraviolet resonance Raman (DUVRR) spectra of solution and solid-state hexahydro-1,3,5-trinitro-1,3,5-triazine (RDX). We also examined the photochemistry of RDX both in solution and solid states. RDX quickly photodegrades with a solution quantum yield of $\varphi \sim 0.35$ as measured by high-performance liquid chromatography (HPLC). New spectral features form over time during the photolysis of RDX, indicating photoproduct formation. The photoproduct(s) show stable DUVRR spectra at later irradiation times that allow standoff detection. In the solution-state photolysis, nitrate is a photoproduct that can be used as a signature for detection of RDX even after photolysis. We used high-performance liquid chromatography–high-resolution mass spectrometry (HPLC-HRMS) and gas chromatography mass spectrometry (GCMS) to determine some of the major solution-state photoproducts. X-ray photoelectron spectroscopy (XPS) was also used to determine photoproducts formed during solid-state RDX photolysis.

Index Headings: **Ultraviolet resonance Raman spectroscopy; UVRRS; Hexahydro-1,3,5-trinitro-1,3,5-triazine photochemistry; RDX photochemistry; HPLC-HRMS; High-performance liquid chromatography–high-resolution mass spectrometry; Standoff detection; Explosives; XPS; X-ray photoelectron spectroscopy.**

INTRODUCTION

Due to the increasing use and risk of improvised explosive devices (IEDs), there is a need for standoff detection methods to detect explosives for security and environmental screening.[1–8] Improvised explosive devices may contain commercial, military, or homemade explosives that make detection challenging.[9] Hexahydro-1,3,5-trinitro-1,3,5-triazine (RDX) is a commonly used explosive. This compound is often found in soil and groundwater near military facilities.[10–12]

Methods for standoff detection must be able to detect trace amounts of explosives at a distance.[3,4,9] Spectroscopy has become a promising method for standoff detection.[1–5,8,10,13,14] Spectroscopic methods can involve irradiating a surface with a laser beam and then collecting the scattered light for analysis.

Raman spectroscopy has been shown to be an effective standoff detection method for explosives.[1–4,8,9] Raman spectroscopy allows for the identification of explosive molecules through their unique vibrational spectra. Normal Raman gives low signal-to-noise (S/N) spectra due to the small Raman cross sections.[1,2,8] Although standoff measurements of explosives have been demonstrated with normal Raman,[3–5,7,9,15] they will be of limited use for standoff detection of low concentrations.

Deep-ultraviolet resonance Raman (DUVRR) spectroscopy is emerging as a promising technique for standoff detection of explosives.[1–3,8,9] Deep-ultraviolet resonance Raman allows for increased sensitivity due to the increased Raman cross sections that result from resonance enhancement. Most explosives have absorption bands in the deep-UV.[1,2,8] Excitation in the deep-UV allows for increased S/N spectra of the explosives making this approach promising for standoff detection.[1,2,8]

With deep-UV excitation into electronic absorption bands, explosive compounds can undergo photolysis leading to a loss of analyte species as well as the appearance of interfering spectral features. These interferences in the DUVRR spectra result from the photodegradation of the analyte to new photochemical products.[16] RDX in both the condensed phase and in the gas phase photodegrades when exposed to UV light into multiple photochemical products.[11,12,17–23] Thus, the DUVRR spectra of RDX may show additional bands that result from photoproducts. These additional bands could result in characteristic DUVRR time-dependent spectra that can be used to identify the explosive precursor.

In this paper, we investigate the photochemistry of solution- and solid-state RDX using 229 nm DUVRR. We determine the solution-state quantum yield for RDX photolysis. We use HPLC-HRMS and gas chromatography mass spectrometry (GCMS) to determine early- and late-stage RDX photoproducts. X-ray photoelectron spectroscopy (XPS) was also used to determine solid-state RDX photoproducts.

EXPERIMENTAL

Raman Measurements. The DUVRR instrumentation was described previously.[24,25] The samples were excited by continuous wave (CW) 229 nm light that was generated by using a Coherent Industries Innova 300 FreD frequency doubled Ar^+ laser.[24] The Raman scattered light was dispersed by using a SPEX Triplemate spectrograph and detected using a Princeton Instruments charge-coupled device camera (Spec-10).

Solution Samples. In the DUVRR photodegradation experiment, 1 mL of a 3 mg/mL RDX (AccuStandard) in CD_3CN (Acros Organics) solution was placed into a 1 cm path length fused silica capped cuvette that was constantly stirred with a magnetic stir bar. The solution was excited with 14 mW of 229 nm light for irradiation times that yielded absorption of 0.1, 1, 2, 5, 10, 20, and 30 photons per molecule. We calculated the number of absorbed photons per molecule using Eq. 1

Received 30 June 2014; accepted 25 November 2014.
* Author to whom correspondence should be sent. E-mail: asher@pitt.edu.
DOI: 10.1366/14-07622

0003-7028/15/6905-0545/0

$$\frac{\text{abs. photons}}{\text{molecule}} = \frac{\left(t_{\text{irrad.}} \times \frac{P_{\text{laser}}}{E_{\text{photon}}}\right)}{N_{\text{init. RDX}}} \quad (1)$$

where P_{laser} is the power of the laser (J/sec), E_{photon} is the energy of a photon (J), $N_{\text{init. RDX}}$ is the number of initial RDX molecules in the sample, and $t_{\text{irrad.}}$ is the irradiation time. We then measured the DUVRR of these samples after these irradiation times by exciting them with ~0.5 mW of 229 nm laser beam focused to a spot size of ~200 μm. Each spectrum was accumulated for 5 min. The deep-ultraviolet Raman of quartz and CD_3CN solvent were subtracted.

The absorbance and high-performance liquid chromatography–high-resolution mass spectrometry (HPLC-HRMS) photodegradation measurements utilized recrystallized RDX (Omni Explosives) dissolved in CD_3CN. This recrystallized RDX was previously extracted from commercial nylon detonating cords (Omni Explosives) and purified by recrystallization from acetonitrile (Fisher Scientific, HPLC Grade).

For the photodegradation absorbance and HPLC-HRMS measurements, 2 mL of the 2 mg/mL RDX in CD_3CN solution was placed in a capped 1 cm path length fused silica cuvette. The solution was stirred continuously with a magnetic stir bar and excited by CW 229 nm light focused to a spot size of ~80 μm. The photolysis is proportional to the average number of absorbed photons per molecule. Here, 100 μL aliquots were taken at varying irradiation times and analyzed by ultraviolet–visible (UV-Vis) spectroscopy and by HPLC-HRMS. The laser power was ~0.5 mW at the sample for exposure times in the early stages of photodegradation (0.01 absorbed photons per molecule). For intermediate exposures (1–2 absorbed photons per molecule), the laser power was increased to ~3.8 mW at the sample. For 5–30 absorbed photons per molecule, the laser power at the sample was increased to ~6.1 mW.

Photodegradation measurements were performed to determine the solution-state photolysis quantum yield for RDX. In this experiment, a 2 mL sample of 0.06 mg/mL RDX in 50/50 methanol/water + 0.1% formic acid solution was placed in a 1 cm path length fused silica cuvette and continuously stirred with a magnetic stirring bar. It was irradiated for a total of 9.5 min by 1 mW of a 229 nm CW laser beam. Here, 100 μL aliquots were taken at 1, 2.8, 5.7, and 9.5 min (2, 6, 12, and 20 absorbed photons per molecule) for HPLC-HRMS measurements.

We measured the DUVRR spectra of neat nitric acid (EMD Chemicals, 69%). A 1 mL sample was irradiated with ~5 mW of a 229 nm CW laser beam. The accumulation time was 90 s per spectrum.

Absorption Measurements. Ultraviolet absorption spectra were measured using a Cary 5000 UV-Vis–near infrared spectrometer operated in a double beam mode. Absorption spectra of the 2 mg/mL RDX irradiated samples were measured in a 0.05 mm path length fused silica cuvette. The sample chamber and spectrometer were purged with N_2 gas (Matheson Tri-Gas) to allow for absorption measurements to 185 nm.

Mass Spectrometry Measurements. High-performance liquid chromatography–high-resolution mass spectrometry measurements were performed using a Dionex UltiMate 3000 Rapid Separation LC System and the Thermo Scientific Q-Exactive mass spectrometer. Electrospray ionization (ESI) in the negative ionization mode was used. An isocratic method utilizing a 50/50 methanol and water and 0.1% formic acid mobile phase was used. The flow rate was 0.2 mL/min.

Here, 100 μL aliquots of RDX solutions at specific exposure times were measured in order to determine photochemical products forming during the photolysis of RDX. A reversed-phase 150 × 2 mm Jupiter column containing 3 μm diameter C-18 silica particles was used. The HRMS mass detection limit is 50 *m*/*z*.

An HPLC-HRMS experiment was also performed to determine the solution-state quantum yield of RDX. A 50 × 2.1 mm Thermo Scientific Hypersil Gold HPLC column with 1.9 μm diameter C-18 silica particles was used. The area of the RDX peak at ~1.5 min was measured in the high-performance liquid chromatography–ultraviolet (HPLC-UV) chromatogram. Calibration standards of 0.06, 0.03, 0.02, 0.008, and 0.004 mg/mL RDX in 50/50 methanol/water and 0.1% formic acid solutions were measured to obtain a calibration curve. Photolyzed RDX samples at varying irradiation times were also measured using the HPLC. The calibration curve was used to determine the concentrations of the irradiated RDX samples. The area of the RDX peak and the concentration of the RDX in the samples were then used to determine the solution photolysis quantum yield.

Gas chromatography mass spectrometry (GCMS) was used to identify formamide in the irradiated 30 photon per molecule irradiated RDX sample in CD_3CN. A GC2010 Shimadzu gas chromatograph coupled with a GCMS-QP2010S Shimadzu mass spectrometer was used for the measurements. A SHRXI-5MS column (30 m in length) was used. The column was held at 50 °C ramped at 10 °C/min to 270 °C and finally ramped to 275 °C with a hold time of 5 min. A volume of 1 μL was injected into the gas chromatograph for each sample. Electron ionization (EI) in the positive ionization mode was used. The scan range was from 30–300 *m*/*z*. The interface and ion source temperatures were held at 280 and 200 °C, respectively. The total run time was 27 min for each sample.

Solid Samples. For the DUVRR solid-state photodegradation experiment, 1 mL of a 1 mg/mL RDX solution in 50:50 CH_3OH:CH_3CN (AccuStandard) was added to MgF_2 powder (Strem Chemicals) and left to evaporate. The dried sample was packed into the groove of a brass rotating Raman cell. The sample was spun during excitation and excited with 4.2 mW of a 229 nm CW laser beam focused to a spot size of ~200 μm. A Teflon DUVRR spectrum was measured for Raman frequency calibration. Each spectrum was accumulated for 5 s.

We prepared solid-state samples for photolysis studies by evaporating 1 mL of a 1 mg/mL RDX solution in 50:50 CH_3OH:CH_3CN (AccuStandard) onto a quartz slide to obtain 1 mg of RDX crystals. Here, 1 μL of a 50:50 H_2O:CH_3OH mixture was added to the 1 mg of RDX crystals on the quartz slide and compacted to form a paste. The system was left to evaporate. The dried sample was irradiated with 8.5 mW of a CW 229 nm laser beam focused to a spot size of ~200 μm. Deep-ultraviolet resonance Raman spectra were accumulated for 30 s.

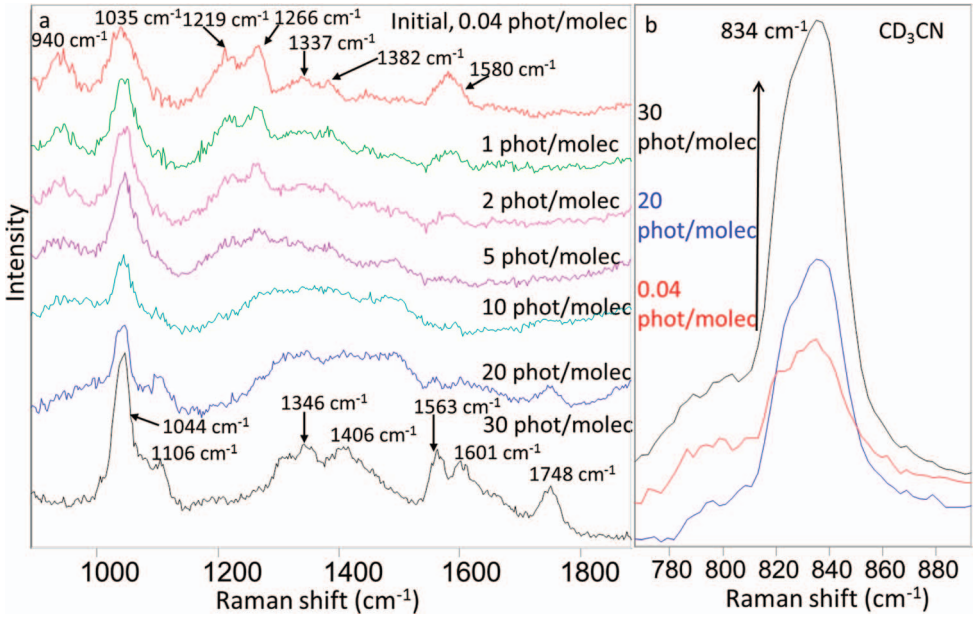

FIG. 1. (**a**) Solution DUVRR spectra of RDX in CD_3CN with increasing irradiation (photons absorbed per molecule). Here, 1 mL of 3 mg/mL RDX in CD_3CN was irradiated with 17 mW of 229 nm light. Quartz and CD_3CN Raman bands were subtracted. (**b**) DUVRR spectra of the 834 cm^{-1} CD_3CN band in the RDX spectra with increasing irradiation time. The CD_3CN band increases in intensity as the photolysis increases.

We prepared a solid-state RDX sample for DUVRR and X-ray photoelectron spectroscopy (XPS) measurements by pipetting 6 μL of water onto a gold-coated glass slide. We then pipetted 10 μL of a 1 mg/mL RDX solution in 50:50 CH_3OH:CH_3CN onto the 6 μL of water on the slide. The system was left to evaporate. The dried sample was irradiated for 465 min with 5 mW CW 229 nm laser beam focused to a spot size of ~300 μm.

X-ray Photoelectron Spectroscopy. X-ray photoelectron spectroscopy (XPS) measurements of the RDX utilized the Thermo Scientific ESCALAB 250Xi instrument with a monochromatic Al Kα source focused to a spot size of 200 μm. The sample stage was cooled with liquid nitrogen in a base vacuum of 1×10^{-10} mbar. A survey spectrum was taken for each sample with a pass energy of 150 eV and a step size of 0.1 eV. The C1s and N1s spectra were measured with a pass energy of 50 eV and a step size of 0.1 eV. The flood gun was used to charge neutralize the RDX sample.

X-ray Powder Diffraction. X-ray powder diffraction was used to determine the crystal structure of the RDX on the SiO_2 substrate and RDX on the gold-coated glass slide. X-ray powder diffraction patterns were collected using a Bruker AXS D8 Discover powder diffractometer with the Lynxeye 1-D detector at 40 kV, 40 mA for Cu Kα ($\lambda = 1.5406$ Å) radiation. A scan speed of 0.40 s/step and a step size of 0.04° was used for the sample of RDX on SiO_2. A scan speed of 5 s/step and a step size of 0.04° was used for the sample of RDX on the gold-coated glass slide. The experimental X-ray powder patterns of RDX for both samples were corrected for background using the Bruker Eva software program. They were then matched to a powder diffraction file (PDF). The experimental RDX X-ray powder patterns are in excellent agreement with the PDF entry 00-044-1619, which is the α form of RDX with unit-cell parameters of a = 13.192, b = 11.592, c = 10.709, and $\alpha = \beta = \gamma = 90°$. See the Supplemental Material for the experimental RDX powder diffraction data.

RESULTS

Solution RDX Photodegradation. The least photolyzed (0.04 photons per molecule) DUVRR spectrum of RDX in Fig. 1a shows DUVRR bands at 940 cm^{-1} (N–N stretching), 1035 cm^{-1} (N–C stretching with CH_2 rocking), 1219 cm^{-1} (N–C stretching), 1266 cm^{-1} (N–N stretching and O–N–O stretching), 1337 cm^{-1} (CH_2 wag or combination), 1382 cm^{-1} (CH_2 twisting), and 1580 cm^{-1} (O–N–O stretching).[1,2,26]

Photochemically induced spectral changes occur even after a small number of photons are absorbed per RDX molecule. This indicates a high RDX photolysis quantum yield. The 940 cm^{-1} N–N stretching band essentially disappears after the absorption of five photons per molecule. This indicates destruction of the RDX N–N bonds in the initial stage of photolysis. The 1580 cm^{-1} band, which derives from O–N–O stretching, also disappears after five photons per molecule illumination. This indicates the loss of the $–NO_2$ groups of RDX.

At longer irradiation times, DUVRR bands of RDX photoproducts appear, as seen in the 20 photons per molecule spectrum. The Raman bands of the photoproducts increase in the 30 photons per molecule spectrum. This is in part due to the absorption decrease at 229 nm observed in the 30 photons per molecule spectrum (Fig. 2a). The photoproducts absorb less at 229 nm, and therefore, a larger volume is excited due to the laser beam penetrating deeper into the solution. This also leads to an increase in the Raman intensities of the solvent Raman bands. Figure 1b shows the increase in Raman intensity of the solvent CD_3CN band at 834 cm^{-1} as the irradiation time increases.

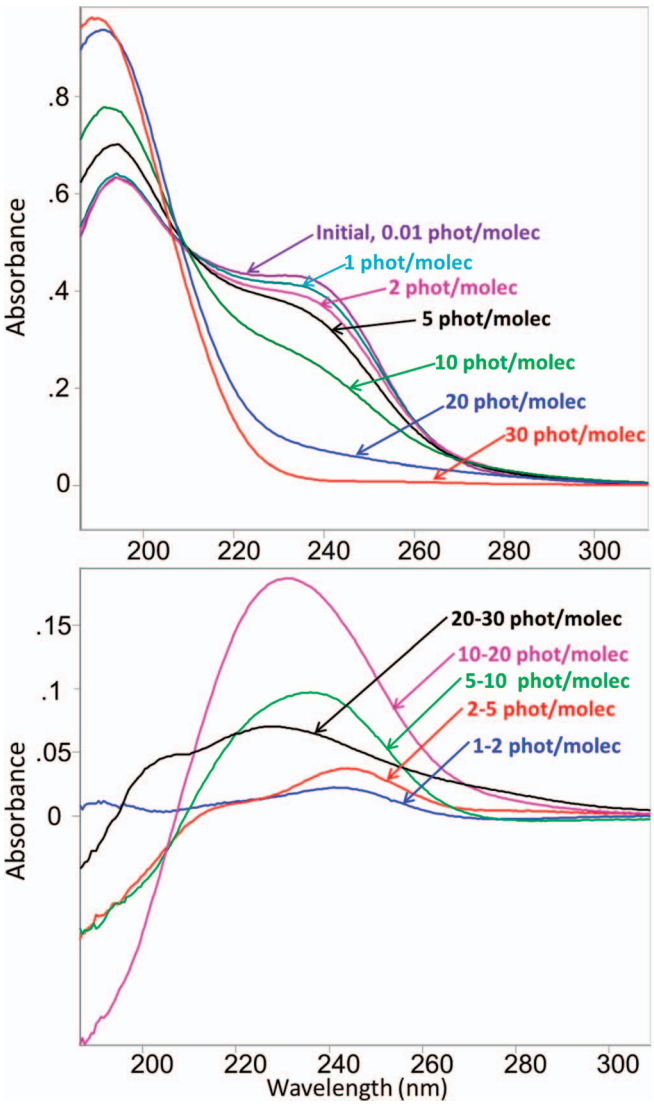

FIG. 2. (**a**) Dependence of the absorption spectra of RDX in CD_3CN upon irradiation of 0.01, 1, 2, 5, 10, 20, and 30 photons per molecule by 229 nm light measured in a 0.05 mm path length cuvette. (**b**) Absorbance difference spectra between 1–2, 2–5, 5–10, 10–20, and 20–30 photons per molecule absorption.

A dominating photoproduct Raman band is seen at 1044 cm^{-1}. This band is likely to result from the ν_1 symmetric stretching vibration of NO_3^-.[27]

Figure 2a shows the dependence of the RDX absorption spectra on increasing irradiation by 229 nm light. The initial RDX absorption spectrum shows a strong peak at ~195 nm and a broad shoulder at ~240 nm. Our recent excited electronic state studies of RDX indicate that these absorption bands derive from multiple overlapping electronic transitions.[28]

The broad absorption shoulder at ~240 nm decreases as RDX is photolyzed. The ~190 nm absorption increases and blue shifts during the photolysis. The 30 photon per molecule spectrum in Fig. 2a shows a single, broad absorption peak with a maximum at ~190 nm. The increase in the 190 nm absorption band observed after long irradiation indicates formation of photoproducts.

A complex behavior is observed in the absorption difference spectra (Fig. 2b). Multiple difference absorption bands evolve during the photolysis. This complex photochemistry is likely due to multiple photoproduct species forming during the photolysis.

We used HPLC-HRMS to determine the photoproducts formed during RDX photolysis (Fig. 3). The HRMS low mass detection limit is 50 *m/z*.

The non-irradiated sample chromatogram shows a peak that elutes at ~3.7 min that derives from the RDX + formate complex. Studies using electrospray ionization (ESI) in the negative ionization mode show that RDX forms adducts with anions.[29] As the irradiation time increases, new peaks appear indicating formation of photoproducts. At least three major condensed phase photoproducts are observed during the initial photolysis with mass-to-charge ratio values of 251, 235, and 219 *m/z*. At larger irradiances (5–30 photons per molecule), an intense peak is observed at ~2.4 min with a mass-to-charge ratio of 62 *m/z*. Table I indicates the Fig. 3 retention times, mass-to-charge ratio values, and their proposed identities.

Three major condensed phase initial photoproducts of RDX are hexahydro-1-nitroso-3,5-dinitro-1,3,5-triazine (MNX), hexahydro-1,3-dinitroso-5-nitro-1,3,5-triazine (DNX), and hexahydro-1,3,5-trinitroso-1,3,5-triazine (TNX) with mass-to-charge ratios of 251, 235, and 219 *m/z*. At five photons per molecule, the nitrate ion appears with a mass-to-charge ratio of 62 *m/z*.

RDX photolysis in the gas phase has been studied in detail.[19–21] Formation of gaseous photoproducts such as NO, N_2O, HCN, and formaldehyde were detected.[19–21]

The photolysis of RDX occurs along multiple parallel photolysis pathways.[11,18,21,30] The DUVRR spectra show resonance-enhanced photoproducts such as nitrate that must involve cleavage of the RDX N–N bonds. The HPLC-HRMS data show the formation of nitroso derivatives as well as formation of nitrate. The DUVRR and HPLC-HRMS give different insights into the complex photolysis of RDX.

Gas chromatography mass spectrometry (GCMS) was used to determine lower molecular weight (<50 *m/z*) compounds formed during RDX photolysis. Figure 4 shows the mass spectrum that identified formamide in the 30 photon per molecule irradiated RDX solution sample. Presumably, we do not see formamide bands present in the photolyzed RDX DUVRR spectra because its concentration is below the detection limit.

We determined the photochemical quantum yield of RDX photolysis in the solution state by monitoring both the RDX peak intensity decrease in the high-performance liquid chromatography (HPLC) and the intensity decrease of the 940 and 1580 cm^{-1} Raman bands as a function of absorbed photons per molecule (Fig. 5).

We use a linear fit of the initial portion of the intensity decay to calculate the slope which indicates the quantum yield (Fig. 5). The initial portion of the 940 and 1580 cm^{-1} Raman peaks intensity decay and the decay of the RDX HPLC peak assumes that at the early stage of photolysis, only RDX molecules absorb photons and photolyze, removing their contributions to the HPLC band and to the RDX Raman intensities.

We measured the HPLC-mass spectrometry to identify the RDX peak and used HPLC-UV chromatograms to determine the RDX content of the initial and the

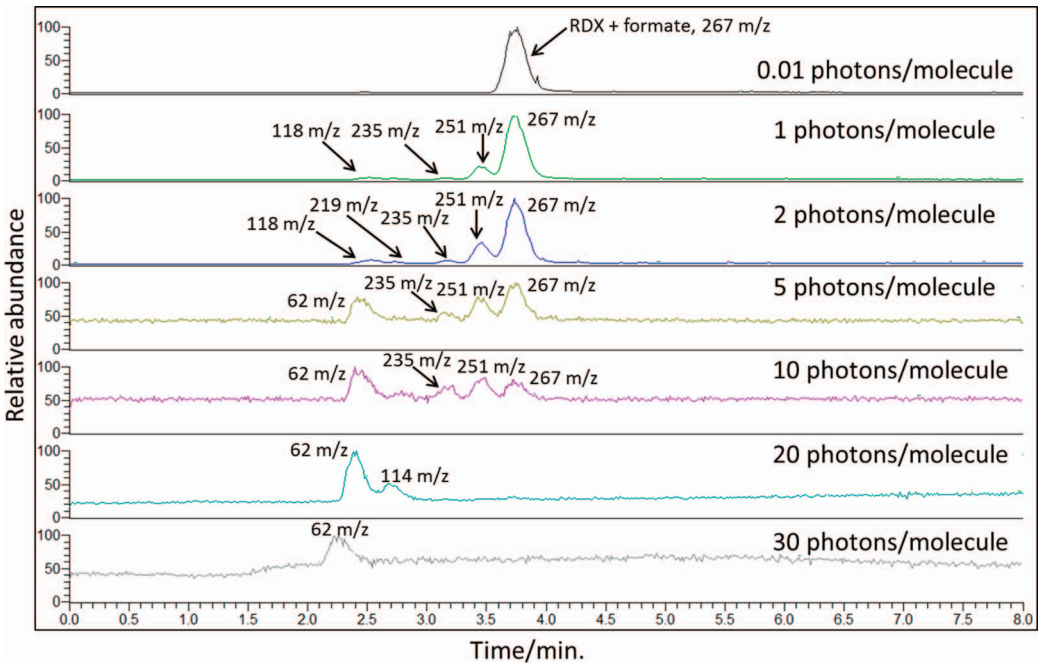

FIG. 3. Mass spectral ion current chromatograms of RDX irradiated by 229 nm light at different irradiation times. The irradiation times are given in the number of absorbed photons per molecule. The mass-to-charge ratio values correspond to the formate adducts. Table I indicates the proposed compounds along with their calculated mass-to-charge ratio values.

TABLE I. Mass chromatogram retention times, mass-to-charge ratio values, empirical formulas, and proposed identities of the species that form a formate adduct.

Retention time/min	*m/z*	Empirical formula	Proposed species/structure + formate
3.7	267	$[C_4H_7O_8N_6]^-$	RDX + formate 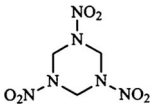
3.5	251	$[C_4H_7O_7N_6]^-$	MNX + formate 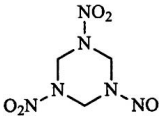
3.2	235	$[C_4H_7O_6N_6]^-$	DNX + formate 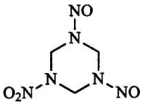
3.0	219	$[C_4H_7O_5N_6]^-$	TNX + formate 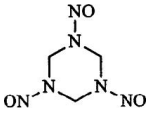
2.3–2.4	62	$[NO_3]^-$	Nitrate

irradiated samples of RDX. We calibrated this measurement with 0.030, 0.015, 0.0076, and 0.0038 mg/mL RDX standard solutions. A linear fit gives a slope indicating a quantum yield of $\varphi \sim 0.35$ ($R^2 = 0.99$).

Figure 5 also shows the intensity decay of the 940 cm^{-1} Raman band vs absorbed photons per molecule in the initial stages of RDX photolysis. The 940 cm^{-1} Raman band derives from N–N stretching[1,2,26] and disappears quickly in the solution-state photolysis, indicating cleavage of the N–NO_2 bond. The linear fit gives a quantum yield of $\varphi = 0.19$ ($R^2 = 0.99$). The intensity decay of the 1580 cm^{-1} O–N–O stretching[1,2,26] Raman band versus absorbed photons per molecule is shown in Fig. 5. The 1580 cm^{-1} Raman band disappears quickly in the solution photolysis. A linear fit gives a quantum yield of $\varphi = 0.32$ ($R^2 = 0.97$).

The DUVRR quantum yield of the 1580 cm^{-1} Raman band is close to that of the HPLC 0.35, while the 940 cm^{-1} Raman band is 0.19. The 940 cm^{-1} Raman band intensity may contain contributions from photoproducts of RDX that will bias the results toward a smaller RDX quantum yield.

We examined the Raman difference spectral changes during photolysis of solution-state RDX to examine

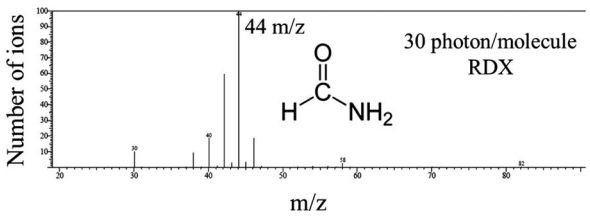

FIG. 4. GCMS of a 30 photon per molecule irradiated RDX sample. The peak at 44 *m/z* is indicative of formamide.

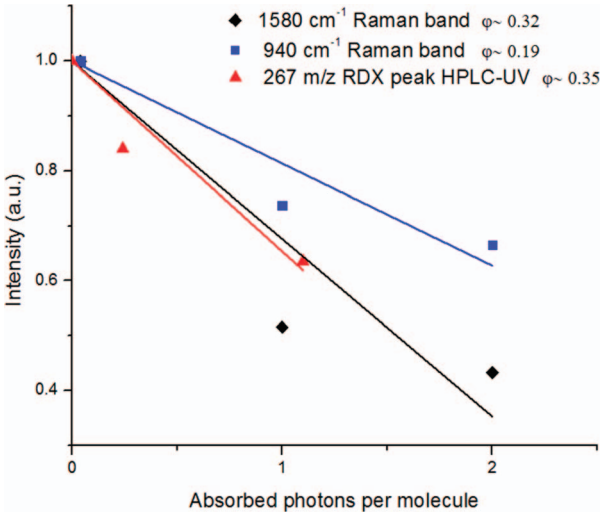

FIG. 5. Solution RDX 940 and 1580 cm^{-1} Raman bands intensity versus absorbed photons per molecule and the 267 *m/z* peak intensity from the HPLC-UV versus absorbed photons per molecule. A linear fit is shown for each of the plots.

photoproduct formation (Fig. 6). In addition, we measured the 229 nm DUVRR spectrum of nitric acid to compare its spectrum to the 30 photon per molecule difference spectrum of RDX (Fig. 6).

Figure 6 compares the RDX initial, 0.04 photon per molecule spectrum to the difference spectra between the initial RDX DUVRR spectrum and the irradiated DUVRR spectra of RDX. Positive features indicate a decrease in the RDX concentrations, while negative features indicate bands from photochemical products. We see negative features showing photoproduct formation at 1346 and 1406 cm^{-1} that increase as the irradiation time increases. The 1044 cm^{-1} Raman band intensity increases with irradiation time, indicating photoproduct formation. The HPLC-HRMS studies discussed above demonstrated the formation of nitrate. We presume that the 1044 cm^{-1} band derives from the NO_3^- symmetric stretching vibration.

Solid RDX Photodegradation. We compared the DUVRR spectra of solid-state RDX (Fig. 7) to that of RDX in CD_3CN (Fig. 1a). We were unable to reliably estimate the number of photons per molecule during the solid-state photolysis of the RDX on the MgF_2 powder.

The minimally photolyzed RDX DUVRR spectra in the solid and solution states are similar and show the same major bands. Deep-ultraviolet resonance Raman bands in the minimally photolyzed 15 s solid-state samples (Fig. 7) are at 762 cm^{-1} (ring bending and NO_2 scissoring), 858 cm^{-1} (C–N stretching with NO_2 scissoring), 940 cm^{-1} (N–N stretching), 1029 cm^{-1} (N–C stretching with CH_2 rocking), 1226 cm^{-1} (N–C stretching), 1269 cm^{-1} (N–N stretching and O–N–O stretching), and 1591 cm^{-1} (O–N–O stretching).[1,2,26]

As solid-state RDX absorbs photons, the isolated 940 cm^{-1} band consisting of N–N stretching decreases and disappears after 1 min of irradiation. This indicates cleavage the N–N bond and the loss of the RDX $-NO_2$ groups. It is known that the initial step in the photochemical decomposition of RDX is the cleavage of the N–N

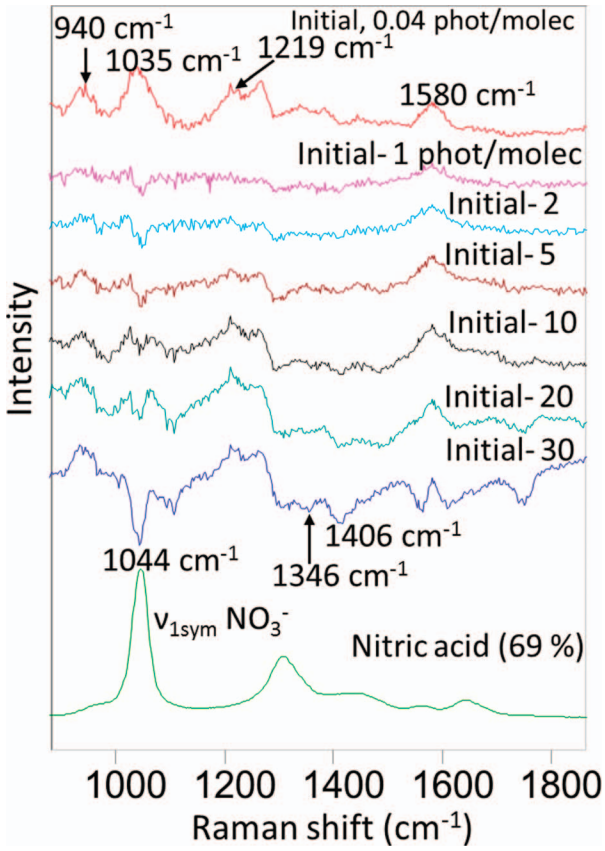

FIG. 6. The RDX CD_3CN initial solution, 0.04 photon per molecule spectrum is shown in comparison to the RDX difference spectra between the minimally photolyzed 0.04 photon per molecule RDX sample, and the 229 nm DUVRR spectra of RDX samples that absorbed 1, 2, 5, 10, 20, and 30 photons per molecule. Negative peaks derive from photoproducts. Here, 229 nm solution DUVRR spectrum of neat nitric acid (69%) is also shown. The quartz and CD_3CN Raman bands were subtracted.

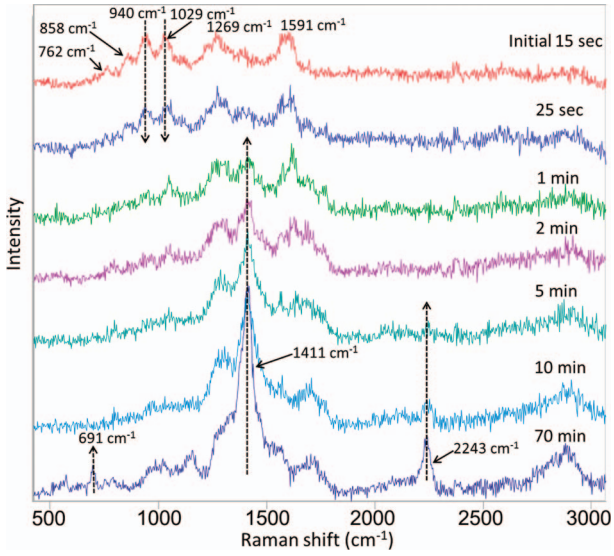

FIG. 7. Irradiation time dependence of 229 nm excited DUVRR spectra of solid-state RDX on MgF_2 powder (<1% by weight RDX). The sample was spun during excitation and irradiated with 4.2 mW of a 229 nm CW laser beam focused to a spot size of ~200 μm.

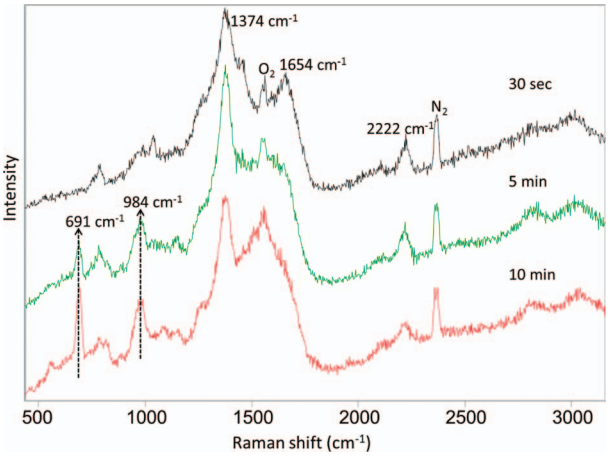

FIG. 8. Here, 229 nm DUVRR spectra of solid-state photolyzed RDX on a SiO_2 substrate with varying irradiation times. The sample was stationary during excitation and contained ~1 mg of RDX. The sample was irradiated with 8.5 mW of a CW 229 nm laser beam focused to a spot size of ~200 μm. The 1555 and 2368 cm^{-1} bands derive from atmospheric oxygen and nitrogen, respectively.

bond to generate NO_2.[19,20,23,30] The solid and solution photolysis of RDX both involve cleavage of the N–N bond releasing NO_2.

A decrease in the 762 and 858 cm^{-1} bands is also seen after 1 min of irradiation, showing the loss of the $–NO_2$ groups. The 1029 cm^{-1} band that involves N–C stretching with CH_2 rocking band disappears after 1 min. The disappearance of this band indicates the loss of the CH_2 groups.

In the 1 min photolyzed RDX spectrum, a band at 1411 cm^{-1} increases in intensity indicating photoproduct formation. The 5 min spectrum shows a band appearing at 2243 cm^{-1} that we assign to C≡N stretching vibration.[31–33] After long irradiation, the 70 min spectrum shows a band at 691 cm^{-1} from a late stage photoproduct.

We studied the later stages of photolysis of RDX to identify late-stage photoproducts that give rise to the 691, 1411, and 2243 cm^{-1} Raman bands present in the 70 min spectrum in Fig. 7. For this sample, ~1 mg of RDX was deposited onto a quartz slide as described above. The sample was stationary during excitation resulting in a faster photolysis and more RDX photodegradation.

The 30 s Fig. 8 DUVRR spectrum of RDX on a SiO_2 substrate displays three strong bands at 1374, 1654, and 2222 cm^{-1}. The band at 2222 cm^{-1} is assigned to a C≡N stretching vibration.[31–33] This band is 20 cm^{-1} downshifted compared to that of RDX on MgF_2 at 2243 cm^{-1}. It appears that two different C≡N containing photochemical products are formed. The C≡N stretching frequency typically occurs between 2200–2260 cm^{-1} in nitrile containing compounds.[34,35] The 1374 and 1654 cm^{-1} bands resemble the "D" and "G" bands of graphitic–amorphous carbon nitride-like samples.[16,31,32,36–38] The 1374 cm^{-1} "D" band is generally observed in graphitic carbon and carbon nitride materials.[37] The ~1650 cm^{-1} "G" band derives from the bond stretching of sp^2 atoms in both ring and chain structures.[31,32] We assign the

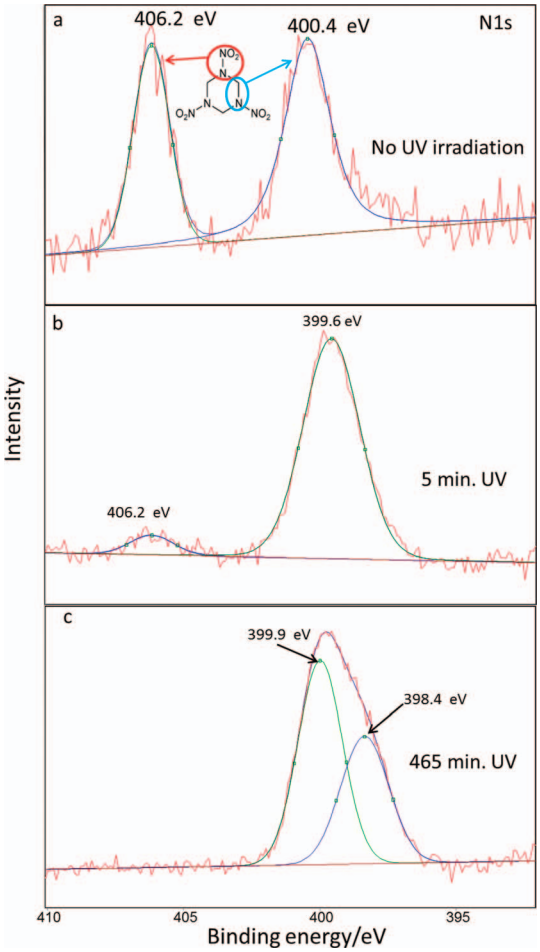

FIG. 9. Nitrogen 1 s electron XPS spectra of RDX (on a gold substrate) at different irradiation times: (**a**) RDX with no UV irradiation, (**b**) RDX after 5 min of UV irradiation, and (**c**) RDX after 465 min of UV irradiation. The spectra were fit to Gaussian bands. The RDX sample was irradiated with 5 mW of a CW 229 nm laser beam focused to a spot size of ~300 μm.

1411 cm^{-1} band to the breathing modes of sp^2 atoms in ring structures.[31,32]

The more extensively irradiated samples show two additional strong peaks at 691 and 984 cm^{-1} that grow in over time. The 984 cm^{-1} peak we assign as a symmetric N-breathing mode of triazine rings due to this being a common vibration seen in graphitic carbon nitrides.[37] The 691 cm^{-1} peak we assign to CNC in plane bending vibrations, which is also seen for carbon nitrides.[37] The 1654 cm^{-1} band becomes more intense as the number of photons absorbed increases. Figure 8 indicates the formation of a graphitic–amorphous carbon nitride after RDX is extensively photolyzed. The carbon nitride DUVRR spectrum can be used as a signature for RDX photochemistry for standoff detection of RDX.

RDX exists in two different polymorphic phases, α-RDX and β-RDX.[26,39–44] We used X-ray diffraction to determine that the RDX on SiO_2 and the RDX on the gold-coated glass slide is in the α-RDX form. We also determined that the RDX on MgF_2 is in the α-RDX form by comparing its UVRR to the normal Raman spectra. The normal Raman spectrum easily differentiates between α-RDX and β-RDX.[26,39,41–44] The α-RDX has molecular symmetry C_s,

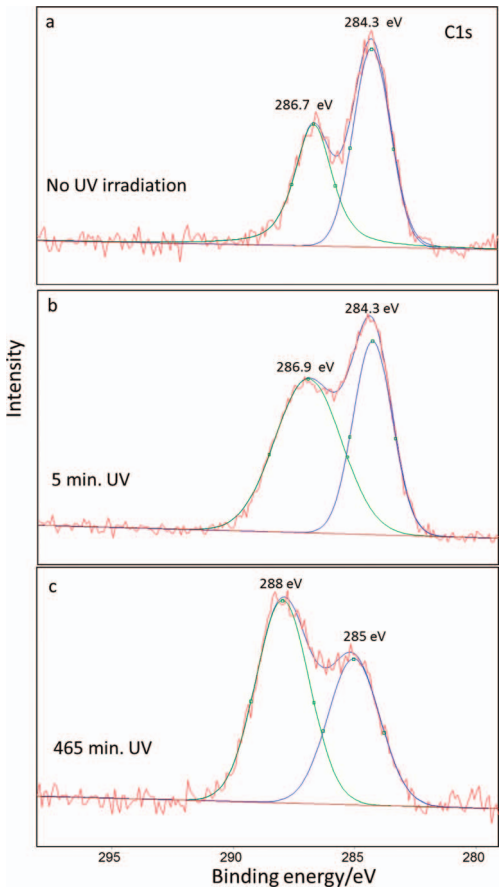

FIG. 10. Carbon 1 s electron XPS spectra of RDX (on a gold substrate) after different irradiation times: (**a**) RDX without UV irradiation, (**b**) RDX with 5 min of UV irradiation, and (**c**) RDX with 465 min of UV irradiation. The spectra were fit to Gaussian bands. The RDX sample was irradiated with 5 mW of a CW 229 nm laser beam focused to a spot size of ~300 μm.

while β-RDX is C_{3v}.[26,41–43] The β-RDX increased molecular symmetry results in a decrease in the number of β-RDX Raman bands.[41–44] We diagnosed that RDX on MgF_2 is α-RDX from the 1595 cm^{-1} (NO_2 asymmetric stretching) and 1032 cm^{-1} (N–C–N stretching) bands present only in α-RDX .[42]

We used X-ray photoelectron spectroscopy (XPS) to study the solid-state RDX photolysis. Deep-ultraviolet resonance Raman and XPS spectra were measured for a ~0.01 mg sample of RDX on a gold-coated glass slide, as discussed above. The DUVRR spectra of this sample resemble that of Fig. 8.

Figure 9a shows two distinct peaks for the N1s electrons of RDX. The peak at 406.2 eV is from the NO_2 group nitrogen electrons.[45,46] The peak at 400.4 eV comes from the ring nitrogen electrons.[45,46] The 406.2 eV peak intensity significantly decreases after 5 min of irradiation and disappears completely after 465 min irradiation, indicating the loss of the $–NO_2$ groups, which is consistent with the DUVRR (Fig. 7). After 5 min irradiation, a peak at 399.6 eV is observed in Fig. 9b that is attributed to sp^2 bonded nitrogen (C=N) electrons.[47–50] After longer irradiation times, the spectrum resembles carbon nitride (Fig. 9c).[47–50] The 398.4 eV peak is assigned to CNC coordinated nitrogen of carbon nitride.[51]

Figure 10a shows two peaks for the C1s electrons of RDX at 286.7 and 284.3 eV that are attributed to sp^3 carbon bonded to nitrogen (C–N) and graphitic carbon, respectively.[49,50] The C1s spectrum changes after irradiation with UV light. Figure 10b shows the 286.9 eV peak, which is assigned to sp^2 bonded carbon (C=N).[48,50] Figure 10c shows a dominant peak at 288 eV, which can be attributed to C–N–C coordination, which is seen in carbon nitride.[51] The C1s and N1s spectra indicate that solid-state RDX photolysis gives rise to carbon nitride-like photoproducts.

CONCLUSION

Solution-state RDX in CD_3CN excited in resonance with 229 nm excitation quickly photolyzes with a quantum yield of $\varphi \sim 0.35$ as determined by HPLC. Deep-ultraviolet resonance Raman spectra show a loss of RDX bands and the appearance of photoproduct bands. The RDX 940 cm^{-1} band, which derives from N–N stretching, decreases and disappears over time, indicating cleavage of the N–N bond. The RDX 1580 cm^{-1} band that involves O–N–O stretching, also decreases and disappears indicating the loss of the $–NO_2$ groups in the initial stages of photolysis. A 1044 cm^{-1} NO_3^- band appears, indicating facile formation of NO_3^-, which can serve as a signature of photolysis of RDX in solution.

We identified some of the solution-state RDX photoproducts. The initial photoproducts are hexahydro-1-nitroso-3,5-dinitro-1,3,5-triazine (MNX), hexahydro-1,3-dinitroso-5-nitro-1,3,5-triazine (DNX), and hexahydro-1,3,5-trinitroso-1,3,5-triazine (TNX). After extensive photolysis, NO_3^- is observed as a photoproduct in solution-state photolysis. Thus, the NO_3^- band can be used as a signature of RDX photolysis in the solution state. The GCMS results show that formamide is also a photoproduct in the later stages of photolysis in the solution state. We do not detect formamide DUVRR spectra.

Solid RDX photodegrades quickly and shows cleavage of the N–N bonds and loss of the $–NO_2$ groups of RDX in the initial photolysis stages. X-ray photoelectron spectroscopy spectra further confirm this loss of $–NO_2$ groups. At late stages in the photolysis of solid-state RDX, the DUVRR spectra show the formation of carbon nitride species. We also do not see formation of NO_3^- in the solid-state photolysis.

ACKNOWLEDGMENTS

We would like to acknowledge Joel Gillespie for facilitating the X-ray photoelectron spectroscopy measurements. We would also like to acknowledge Steven Geib for the X-ray powder diffraction measurements. This work was funded by the Office of Naval Research (ONR) N00014-12-1-0021 contract.

SUPPLEMENTAL MATERIAL

All supplemental material mentioned in the text, including two figures and a description of the figures, is available in the online version of the journal at http://www.s-a-s.org.

1. D.D. Tuschel, A.V. Mikhonin, B.E. Lemoff, S.A. Asher. "Deep Ultraviolet Resonance Raman Excitation Enables Explosives Detection". Appl. Spectrosc. 2010. 64(4): 425-432.

2. M. Ghosh, L. Wang, S.A. Asher. "Deep-Ultraviolet Resonance Raman Excitation Profiles of NH_4NO_3, PETN, TNT, HMX, and RDX". Appl. Spectrosc. 2012. 66(9): 1013-1021.
3. H. Östmark, M. Nordberg, T.E. Carlsson. "Stand-off Detection of Explosives Particles by Multispectral Imaging Raman Spectroscopy". Appl. Opt. 2011. 50(28): 5592-5599.
4. J.C. Carter, S.M. Angel, M. Lawrence-Snyder, J. Scaffidi, R.E. Whipple, J.G. Reynolds. "Standoff Detection of High Explosive Materials at 50 Meters in Ambient Light Conditions Using a Small Raman Instrument". Appl. Spectrosc. 2005. 59(6): 769-775.
5. L. Pacheco-Londoño, W. Ortiz-Rivera, O. Primera-Pedrozo, S. Hernández-Rivera. "Vibrational Spectroscopy Standoff Detection of Explosives". Anal. Bioanal. Chem. 2009. 395(2): 323-335.
6. D.S. Moore. "Instrumentation for Trace Detection of High Explosives". Rev. Sci. Instrum. 2004. 75(8): 2499-2512.
7. D. Moore. "Recent Advances in Trace Explosives Detection Instrumentation". Sens. Imaging. 2007. 8(1): 9-38.
8. K.L. Gares, S.V. Bykov, B. Godugu, S.A. Asher. "Solution and Solid Trinitrotoluene (TNT) Photochemistry: Persistence of TNT-like Ultraviolet (UV) Resonance Raman Bands". Appl. Spectrosc. 2014. 68(1): 49-56.
9. A. Pettersson, I. Johansson, S. Wallin, M. Nordberg, H. Östmark. "Near Real-Time Standoff Detection of Explosives in a Realistic Outdoor Environment at 55 m Distance". Propellants, Explos., Pyrotech. 2009. 34(4): 297-306.
10. N.A. Hatab, G. Eres, P.B. Hatzinger, B. Gu. "Detection and Analysis of Cyclotrimethylenetrinitramine (RDX) in Environmental Samples by Surface-Enhanced Raman Spectroscopy". J. Raman Spectrosc. 2010. 41(10): 1131-1136.
11. G.R. Peyton, M.H. LeFaivre, S. Maloney. "Verification of RDX Photolysis Mechanism". Champaign, IL: US Army Corps of Engineers, Engineer Research and Development Center, Construction Engineering Research Laboratory, 1999. Pp. 1-58.
12. J. Hawari, A. Halasz, C. Groom, S. Deschamps, L. Paquet, C. Beaulieu, A. Corriveau. "Photodegradation of RDX in Aqueous Solution: A Mechanistic Probe for Biodegradation with Rhodococcus sp". Environ. Sci. Technol. 2002. 36(23): 5117-5123.
13. B. Zachhuber, C. Gasser, G. Ramer, E. t. H. Chrysostom, B. Lendl. "Depth Profiling for the Identification of Unknown Substances and Concealed Content at Remote Distances Using Time-Resolved Stand-Off Raman Spectroscopy". Appl. Spectrosc. 2012. 66(8): 875-881.
14. H.-B. Liu, Y. Chen, G.J. Bastiaans, X.C. Zhang. "Detection and Identification of Explosive RDX by THz Diffuse Reflection Spectroscopy". Opt. Express. 2006. 14(1): 415-423.
15. S. Wallin, A. Pettersson, H. Östmark, A. Hobro. "Laser-Based Standoff Detection of Explosives: A Critical Review". Anal. Bioanal. Chem. 2009. 395(2): 259-274.
16. L. Wang, D. Tuschel, S.A. Asher. "229 nm UV Photochemical Degradation of Energetic Molecules". Proc. SPIE. 2011. 80181B-1-80181B-6.
17. T.L. Andrew, T.M. Swager. "Detection of Explosives via Photolytic Cleavage of Nitroesters and Nitramines". J. Org. Chem. 2011. 76(9): 2976-2993.
18. D.J. Glover, J.C. Hoffsommer. "Photolysis of RDX in Aqueous Solution, With and Without Ozone". Naval Surface Weapons Center White Oak, Silver Spring, MD: Research and Technology Dept, 1979.
19. Y.Q. Guo, M. Greenfield, E.R. Bernstein. "Decomposition of Nitramine Energetic Materials in Excited Electronic States: RDX and HMX". J. Chem. Phys. 2005. 122(24): 244310.
20. M. Greenfield, Y.Q. Guo, E.R. Bernstein. "Ultrafast Photodissociation Dynamics of HMX and RDX from Their Excited Electronic States via Femtosecond Laser Pump–probe Techniques". Chem. Phys. Lett. 2006. 430(4–6): 277-281.
21. A.F. Smetana, S. Bulusu. "Photochemical Studies of Secondary Nitramines. Part 2. Ultraviolet Photolysis and Ozonolysis of RDX in Aqueous Solutions". No. ARLCD-TR-77039-PT-2. Army Armament Research and Development Center, Dover, New Jersey, Large Caliber Weapon Systems Lab, 1977.
22. Y.Q. Guo, M. Greenfield, A. Bhattacharya, E.R. Bernstein. "On the Excited Electronic State Dissociation of Nitramine Energetic Materials and Model Systems". J. Chem. Phys. 2007. 127(15): 154301.
23. H.-S. Im, E.R. Bernstein. "On the Initial Steps in the Decomposition of Energetic Materials from Excited Electronic States". J. Chem. Phys. 2000. 113(18): 7911-7918.
24. S.A. Asher, R.W. Bormett, X.G. Chen, D.H. Lemmon, N. Cho, P. Peterson, M. Arrigoni, L. Spinelli, J. Cannon. "UV Resonance Raman Spectroscopy Using a New cw Laser Source: Convenience and Experimental Simplicity". Appl. Spectrosc. 1993. 47(5): 628-633.
25. S. Bykov, I. Lednev, A. Ianoul, A. Mikhonin, C. Munro, S.A. Asher. "Steady-State and Transient Ultraviolet Resonance Raman Spectrometer for the 193-270 nm Spectral Region". Appl. Spectrosc. 2005. 59(12): 1541-1552.
26. Z.A. Dreger, Y.M. Gupta. "High Pressure Raman Spectroscopy of Single Crystals of Hexahydro-1,3,5-trinitro-1,3,5-triazine (RDX)". J. Phys. Chem. B. 2007. 111(15): 3893-3903.
27. S.A. Asher, D.D. Tuschel, T.A. Vargson, L. Wang, S.J. Geib. "Solid State and Solution Nitrate Photochemistry: Photochemical Evolution of the Solid State Lattice". J. Phys. Chem. A. 2011. 115(17): 4279-4287.
28. W.A. Al-Saidi, S.A. Asher, P. Norman. "Resonance Raman Spectra of TNT and RDX Using Vibronic Theory, Excited-State Gradient, and Complex Polarizability Approximations". J. Phys. Chem. A. 2012. 116(30): 7862-7872.
29. A. Gapeev, M. Sigman, J. Yinon. "Liquid Chromatography/Mass Spectrometric Analysis of Explosives: RDX Adduct Ions". Rapid Commun. Mass Spectrom. 2003. 17(9): 943-948.
30. N.J. Harris, K. Lammertsma. "Ab Initio Density Functional Computations of Conformations and Bond Dissociation Energies for Hexahydro-1,3,5-trinitro-1,3,5-triazine". J. Am. Chem. Soc. 1997. 119(28): 6583-6589.
31. A.C. Ferrari, S.E. Rodil, J. Robertson. "Interpretation of Infrared and Raman Spectra of Amorphous Carbon Nitrides". Phys. Rev. B. 2003. 67(15): 155306.
32. S.E. Rodil, A.C. Ferrari, J. Robertson, S. Muhl. "Infrared Spectra of Carbon Nitride Films". Thin Solid Films. 2002. 420–421: 122-131.
33. A.K.M.S. Chowdhury, D.C. Cameron, M.S.J. Hashmi. "Vibrational Properties of Carbon Nitride Films by Raman Spectroscopy". Thin Solid Films. 1998. 332(1–2): 62-68.
34. G. Socrates. Infrared and Raman Characteristic Group Frequencies: Tables and Charts. Chichester, West Sussex: John Wiley and Sons Ltd., 2004.
35. N.B. Colthup, L.H. Daly, S.E. Wiberley. Introduction to Infrared and Raman Spectroscopy. San Diego, CA: Academic Press, 1990. 3rd ed.
36. H.X. Zhang, H.Y. Li, P.X. Feng. "Nanostructured Carbon Nitride Films Deposited Using The Low-Cost Penning Discharge Plasma-Sputtering Technique". Int. J. Mod. Phys. B. 2008. 22(23): 3957-3966.
37. P.F. McMillan, V. Lees, E. Quirico, G. Montagnac, A. Sella, B. Reynard, P. Simon, E. Bailey, M. Deifallah, F. Corà. "Graphitic Carbon Nitride $C_6N_9H_3$·HCl: Characterisation by UV and Near-IR FT Raman Spectroscopy". J. Solid State Chem. 2009. 182(10): 2670-2677.
38. S.S. Roy, R. McCann, P. Papakonstantinou, P. Maguire, J.A. McLaughlin. "The Structure of Amorphous Carbon Nitride Films Using a Combined Study of NEXAFS, XPS and Raman Spectroscopies". Thin Solid Films. 2005. 482(1–2): 145-150.
39. E.D. Emmons, M.E. Farrell, E.L. Holthoff, A. Tripathi, N. Green, R.P. Moon, J.A. Guicheteau, S.D. Christesen, P.M. Pellegrino, A.W. Fountain, III. "Characterization of Polymorphic States in Energetic Samples of 1,3,5-Trinitro-1,3,5-Triazine (RDX) Fabricated Using Drop-on-Demand Inkjet Technology". Appl. Spectrosc. 2012. 66(6): 628-635.
40. I.G. Goldberg, J.A. Swift. "New Insights into the Metastable β Form of RDX". Cryst. Growth Des. 2012. 12(2): 1040-1045.
41. R.J. Karpowicz, T.B. Brill. "Comparison of the Molecular Structure of Hexahydro-1,3,5-trinitro-s-triazine in the Vapor, Solution and Solid Phases". J. Phys. Chem. 1984. 88(3): 348-352.
42. R. Infante-Castillo, L.C. Pacheco-Londoño, S.P. Hernández-Rivera. "Monitoring the α→β Solid–Solid Phase Transition of RDX with Raman Spectroscopy: A Theoretical and Experimental Study". J. Mol. Struct. 2010. 970(1–3): 51-58.
43. B.M. Rice, C.F. Chabalowski. "Ab Initio and Nonlocal Density Functional Study of 1,3,5-Trinitro-s-triazine (RDX) Conformers". J. Phys. Chem. A. 1997. 101(46): 8720-8726.
44. P. Torres, L. Mercado, I. Cotte, S.P. Hernández, N. Mina, A. Santana, R.T. Chamberlain, R. Lareau, M.E. Castro. "Vibrational Spectroscopy Study of β and α RDX Deposits". J. Phys. Chem. B. 2004. 108(26): 8799-8805.
45. F.J. Owens, J. Sharma. "X-Ray Photoelectron Spectroscopy and Paramagnetic Resonance Evidence for Shock-induced Intramolec-

ular Bond Breaking in Some Energetic Solids". J. Appl. Phys. 1980. 51(3): 1494-1497.
46. C.M. Mahoney, A.J. Fahey, K.L. Steffens, B.A. Benner, R.T. Lareau. "Characterization of Composition C4 Explosives Using Time-of-Flight Secondary Ion Mass Spectrometry and X-ray Photoelectron Spectroscopy". Anal. Chem. 2010. 82(17): 7237-7248.
47. M. Aono, S. Aizawa, N. Kitazawa, Y. Watanabe. "XPS Study of Carbon Nitride Films Deposited by Hot Filament Chemical Vapor Deposition Using Carbon Filament". Thin Solid Films. 2008. 516(5): 648-651.
48. E. Ech-chamikh, A. Essafti, Y. Ijdiyaou, M. Azizan. "XPS Study of Amorphous Carbon Nitride (a-C:N) Thin Films Deposited by Reactive RF Sputtering". Sol. Energy Mater. Sol. Cells. 2006. 90(10): 1420-1423.
49. M. Kim, S. Hwang, J.-S. Yu. "Novel Ordered Nanoporous Graphitic C3N4 as a Support For Pt-Ru Anode Catalyst in Direct Methanol Fuel Cell". J. Mater. Chem. 2007. 17(17): 1656-1659.
50. M. Matsuoka, S. Isotani, R.D. Mansano, W. Sucasaire, R.A. Pinto, J.C. Mittani, K. Ogata, N. Kuratani. "X-Ray Photoelectron Spectroscopy and Raman Spectroscopy Studies on Thin Carbon Nitride Films Deposited by Reactive RF Magnetron Sputtering". World J. Nano Sci. Eng. 2012. 2(2): 92-102.
51. A. Thomas, A. Fischer, F. Goettmann, M. Antonietti, J.-O. Müller, R. Schlögl, J.M. Carlsson. "Graphitic Carbon Nitride Materials: Variation of Structure and Morphology and Their Use as Metal-free Catalysts". J. Mater. Chem. 2008. 18(41): 4893-4908.